Ozone profile retrieval from GOMOS limb scattering measurements

Ghassan Taha,[1] Glen Jaross,[1] Didier Fussen,[2] Filip Vanhellemont,[2] Erkki Kyrölä,[3] and Richard D. McPeters[4]

Received 21 September 2007; revised 25 July 2008; accepted 24 September 2008; published 10 December 2008.

[1] We analyzed a set of Global Ozone Monitoring by Occultation of Stars (GOMOS) bright limb measurements with solar zenith angles less than 85° and within 150 km of Stratospheric Aerosol and Gas Experiment II (SAGE II) measurements. In order to perform any species retrieval, GOMOS measurements were first corrected for stray light contamination. GOMOS pointing was analyzed using scene-based tangent height algorithms, and the best results were achieved using ~350 nm (Rayleigh) pixels that were consistent with GOMOS known accurate pointing. In order to demonstrate GOMOS bright limb capabilities, ozone profile retrievals were performed using GOMOS measurements of limb-scattered radiances with the Ozone Mapping and Profiler Suite limb profiler algorithm. The algorithm performs a simultaneous optimal estimation inversion of both Hartley-Huggins and Chappuis band radiances. We restricted our GOMOS ozone retrievals to the range 25–53 km, a region of relatively constant measurement uncertainty. In this first look at GOMOS limb data, the retrieved ozone profiles agree with collocated SAGE II measurements on average to within 10–15% and with a standard deviation of 10%. Retrieval results were consistent for both upper and lower GOMOS detector bands.

Citation: Taha, G., G. Jaross, D. Fussen, F. Vanhellemont, E. Kyrölä, and R. D. McPeters (2008), Ozone profile retrieval from GOMOS limb scattering measurements, *J. Geophys. Res.*, *113*, D23307, doi:10.1029/2007JD009409.

1. Introduction

[2] The Global Ozone Monitoring by Occultation of Stars experiment (GOMOS) onboard Envisat is designed to measure stellar occultation at wavelengths from the near-UV through the near-IR region and produces profiles of O_3, NO_2, NO_3, OClO, and aerosol extinction as standard products [*Kyrölä et al.*, 2004]. In order to distinguish stellar light from the sky background under conditions where the Earth limb is also illuminated by the Sun, the detector measures the background spectrum just above and below each star as the sensor tracks its movement through the limb [*European Space Agency* (*ESA*), 2007a]. If properly calibrated, limb-scattered (LS) radiances measured by GOMOS can be used to retrieve various gaseous species and aerosol extinction. The information content is similar to that obtained by other limb scatter sensors, such as the Scanning Imaging Absorption Spectrometer for Atmospheric Cartography (SCIAMACHY) on Envisat [*Bovensmann et al.*, 1999], the Optical Spectrograph and Infrared Imager System (OSIRIS) on Odin [*Llewellyn et al.*, 2004], and the Stratospheric Aerosol and Gas Experiment III (SAGE III) [*Rault*, 2005], with one important difference; each GOMOS spectrum contains a stellar signal. Sensor pointing, and, hence, the vertical registration of atmospheric species profiles, should be superior to other limb sensors.

[3] The main objective of this work is to demonstrate the capability of GOMOS bright limb measurements for ozone profiles retrievals. This work will also exploit GOMOS known accurate pointing to evaluate scene-based altitude registration approaches planned for the Ozone Mapping and Profiler Suite (OMPS) limb profiler [*Flynn et al.*, 2006]. OMPS is scheduled to fly onboard the National Polar Orbiting Operational Environmental Satellite System Preparatory Project satellite in 2010.

[4] The instrument measures the stellar occultation under three different conditions: dark, twilight, and bright limb. Occultation retrievals in the bright limb where the solar zenith angle (SZA) is less than 97° are very difficult because of the strong solar light interference and often produce a poor quality ozone profile [*Meijer et al.*, 2004]. On the other hand, background limb measurements for the same bright conditions are ideal for ozone retrieval by the LS technique and can therefore supplement the GOMOS planned global coverage. The GOMOS measurement principle is shown in Figure 1. Incoming photons from approximately 5 km above and below the star are imaged in one dimension, and dispersed spectrally across the other dimension, of the charge-coupled device detector. Spectrally resolved LS signals above and below the star are separately integrated over their narrow vertical ranges. As with the stellar occultation data, a set of measurements comprising a

[1] Science Systems and Applications Inc., Lanham, Maryland, USA.
[2] Belgian Institute for Space Aeronomy, Brussels, Belgium.
[3] Finnish Meteorological Institute, Helsinki, Finland.
[4] NASA Goddard Space Flight Center, Laboratory for Atmospheres, Greenbelt, Maryland, USA.

0148-0227/08/2007JD009409

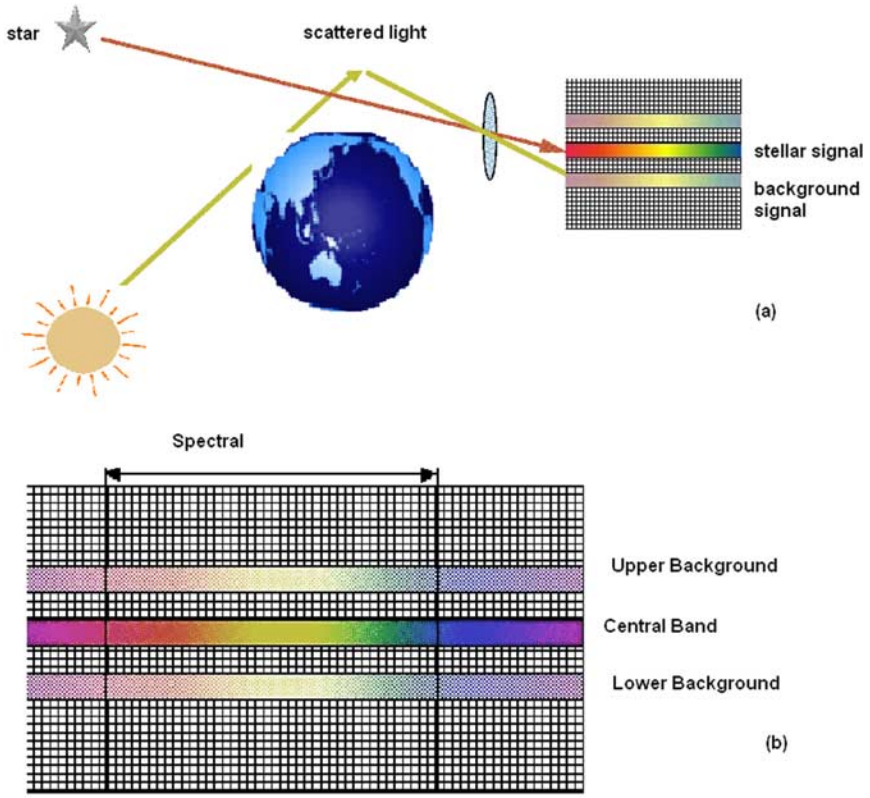

Figure 1. (a) Schematic diagram that illustrates GOMOS measurement methodology. It mainly performs stellar occultation measurements to detect the atmospheric transmission spectrum between the star and the instrument. On the dayside bright limb, GOMOS will also detect unwanted scattered solar light. (b) Three GOMOS bands of charge-coupled device array measured by the spectrometer (7 pixels each) imaged in the vertical direction and spectrally dispersed horizontally. The targeted star signal is then corrected by removing the background component. On the other hand, when properly calibrated, the two background signals can be converted to limb radiance spectrum [*ESA*, 2007a].

single profile is obtained as the star rises or sets through the limb.

[5] In this paper, we analyze a set of 98 bright limb GOMOS profiles during 2003, which were selected to be within 150 km and on the same day as Stratospheric Aerosol and Gas Experiment II (SAGE II) measurements. Measurements were randomly selected, and analysis of the whole preselected data set is presented in this paper. Section 2 provides a brief description and assessment of GOMOS limb scattering measurement. In section 3, we analyze stray light contamination and describe a correction method used for removing this signal. Section 4 analyzes GOMOS tangent height registration using scene-based algorithms. In section 5 we describe the algorithm used for ozone profile retrieval. In section 6, we present and discuss the first results of the GOMOS limb scattering retrieved ozone profile by comparing it with SAGE II measurements. Finally, summary and conclusions of this study are presented in section 7.

2. Measurement Quality

[6] The GOMOS level 1b LS signals are decoded using the following expression:

$$\text{signal} = \text{offset} + \text{digital number}/\text{gain},$$

where the signal is in electrons. Values of offset and gain are stored in each file. The decoded spectra obtained in electrons are converted into units of radiance (ph/s/cm^2/nm/sr) using the radiometric sensitivity curves for background signal. These curves, which vary in wavelength, are given for each occultation as lookup tables [*ESA*, 2007a]. More details of the measurement calibration can also be found in work by *ESA* [2007b]. Standard geolocation parameters, latitude, longitude, and SZA are provided in the level 1b data product at the tangent point for each upper and lower background profile. The tangent point is the location in the atmosphere where, ignoring scattering, photons traced back from the sensor would have their closest approach to the Earth's surface.

[7] Figure 2a shows a sample of GOMOS-calibrated limb radiances plotted at selected wavelengths that are relevant to ozone retrieval, measured on 7 August 2003 (latitude = 46.55°, longitude = −2.22°, and SZA = 43.12°). The radiances are colored for different wavelengths, from 280 nm (black) to 755 nm (red). Radiances at each wavelength are for upper (dash-dotted) and lower (solid) bands. Notice the good agreement between the upper and lower profiles. Close investigation of the sample radiances reveal several features that persist in all data sets investigated in this study. Limb measurements usually do not extend below ~20 km. Measurements at ~280 nm are very noisy as a

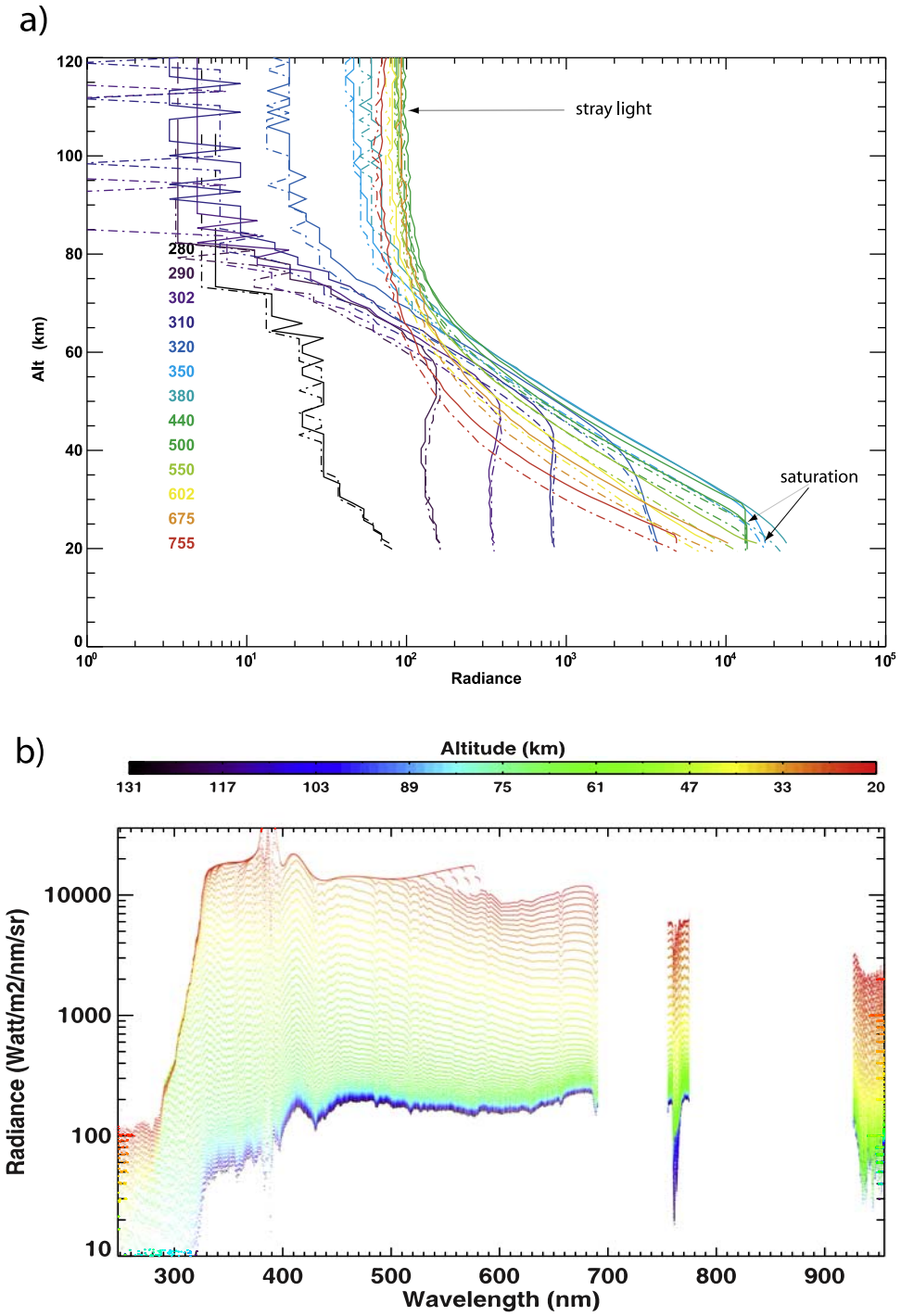

Figure 2. (a) Sample of GOMOS-calibrated radiances at wavelengths of 280–755 nm measured on 7 August 2003 (latitude = 46.55°, longitude = −2.22°, and SZA = 43.12°). Radiances at each wavelength are for upper (dash-dotted) and lower (solid) bands. (b) GOMOS-calibrated radiances spectral measurements colored by altitude.

result of the weak signal at short wavelengths. This weakness manifests itself as large stepwise digitization errors seen in Figure 2a. Also, radiances suffer from detector saturation due to strong signal at lower altitudes, usually below 25 km and mostly for wavelengths between 400 and 600 nm. The most challenging issue is stray light contamination. Stray light contamination in LS measurements is often caused by light internally scattered into the field of view from lower altitudes [*Rault*, 2005]. At 300 nm and shorter, where stray light from longer wavelengths is sometimes also significant, the contamination appears to be in band and minimal except at the lowest altitudes. This suggests that the GOMOS spectrometer has no serious problem with out-of-band stray light. Out-of-band or spec-

tral stray light usually takes place when a light at a certain wavelength is scattered to a pixel that belongs to a different wavelength. At long wavelengths, where the light penetrates into the lower atmosphere, the stray light signature is more pronounced. Figure 2b shows GOMOS spectra for the same event, colored by altitude, starting from 20 (red) to 131 km (black). No correction for stray light has been performed on these spectra. The radiances show obvious atmospheric signatures, such as the O_2 A band around 761 nm, which varies little with altitude. Spectra at high altitudes (>80 km) usually exhibit few atmospheric characteristics. The O_2 A band itself should be seen in emission at higher altitude but appears as an absorption feature because of the dominance of stray light in the signal. In-band light originating from below the instantaneous field of view (IFOV) and scattering in the instrument's optics is the most plausible source for the enhanced signals at high altitude. The photometer IFOV is 140 arcsec vertically (spatial) and 50 arcsec horizontally (spectral). Integration time is 0.498 s ± 0.05 ms.

3. Stray Light Analysis and Removal

[8] The first and most significant step in retrieving species using GOMOS limb measurements is to model and remove the stray light signal. *Rault* [2005] successfully estimated and corrected stray light contamination that was affecting SAGE limb measurements and subsequently retrieved a good quality ozone profile [*Rault and Taha*, 2007]. For our work, forward model calculations were carried out using a radiative transfer model [*Herman et al.*, 1995] so as to accurately model limb scattering radiances at the GOMOS measurement location and characterize stray light signals. Our implementation of the model used inputs from nearby SAGE II O_3, NO_2, and aerosol profiles, as well as the National Centers for Environmental Prediction temperatures and pressures that accompany the SAGE files. We assumed that stratospheric aerosols were composed of sulfates. Radiance profiles were constructed at selected pixels relevant to the retrieval algorithm and compared to GOMOS measurements. Figure 3a is an example of such a comparison that illustrates the extent of the stray light contamination at 602 nm. Figure 3a is a plot of uncorrected measurements (red) and calculated radiance (black). Figure 3b contains the percent difference between the calculated and measured upper (blue) and lower (green) band radiances. There is an obvious disagreement above 30 km that gradually increases with altitude. Below 30 km, the disagreement is smaller, within 15–20%. To model the stray light signal, we must first assume that signals between 80 and 120 km are entirely stray light and are significantly above the noise floor. As discussed by *Rault* [2005], the sensor response to a point source, referred to as its point spread function (PSF), has tails extending far above and below the point. Unless the GOMOS sensor is thought to have an unusual ghost problem, the tails of point spread functions can be represented well with a low-order polynomial function. Lacking published measurements of vertical PSF, there is no way to account for the out-of-field light, and only an empirical correction can be used. For that purpose, a linear fit that pairs the measured radiance and altitude by minimizing the chi-square was used to model the 80–120 km signal, which is a complex combination of radiance profiles and point spread functions. We extend the fit results to lower altitudes in order to estimate stray light (violet), as seen in Figure 3c. The stray light estimate is subtracted from the GOMOS upper (red dash-dotted) and lower (red solid) measurements. Stray light estimates are similar to those made by *Rault* [2005]. Figure 3d is a plot of the difference between GOMOS upper and lower bands after stray light correction. The upper-lower difference is mainly a consistency test to verify that applied corrections are consistent for both bands. The upper-lower difference is less than 5%, up to 65 km, before (Figure 3b) and after applying stray light corrections (Figure 3d). Figure 3d shows good agreement between the calculated radiance and both corrected measurements, within 10% at an altitude range of 25–65 km. GOMOS absolute calibration errors and possible inaccurate instrument model assumptions, as well as the true state of atmosphere uncertainties, can explain the observed 10% difference. Also shown in Figure 3d are the normalized radiance differences (dash-dotted). Radiances normalized to their value at 45.5 km are used in the retrieval algorithm, mainly to reduce the impact of reflectivity, cloud effects, and instrument calibration (see section 5). Figure 3b shows that normalization does indeed reduce the difference between the measured upper and lower bands and the modeled radiance to within 2–3%. There is a small but noticeable structure around 32 km, which is unrelated to stray light contamination. This example demonstrates that the stray light corrections are adequately accounting for most of the stray light signal in both bands up to 60 km. Stray light contamination is very small at UV wavelengths, possibly because at these wavelengths, the ozone layer is acting as a shield from the upwelling radiance from below, the likely source of stray light.

[9] The procedures described above were applied to estimate and correct for the stray light signal independently at each wavelength. Notice that only measured radiances were used to model and subsequently correct for stray light signal. The calculated radiances generated by the forward model and described above are only used to validate these corrections. Figure 4 is a plot of the mean difference (98 events) of measured and calculated altitude-normalized radiances at 350, 500, 602, and 670 nm (solid) and the standard deviation of the means (dash-dotted). The numbers shown in the top left corner are the mean difference over the altitude range 22–50 km. There is excellent agreement between modeled and measured radiances, within 2–3%, below 50 km. The standard deviation is comparable to the difference, a sign of small spread of these differences. The differences are mainly caused by modeling and instrumental errors. Above 35 km, where stray light at longer wavelengths is significant, the difference is even smaller, indicating sufficient corrections to within 2%. There is a noticeable structure that peaks near 32 km and has an amplitude that increases with wavelength. The same feature can also be seen in Figure 3d. Increased standard deviation for the same altitude region means more variability. This structure results from the use of constant surface albedo of $A = 0.1$ in the forward model. In reality, reflecting surfaces are more heterogeneous, and their contribution to the observed limb signal varies by location and altitude. Larger differences below 25 km, caused by signal satura-

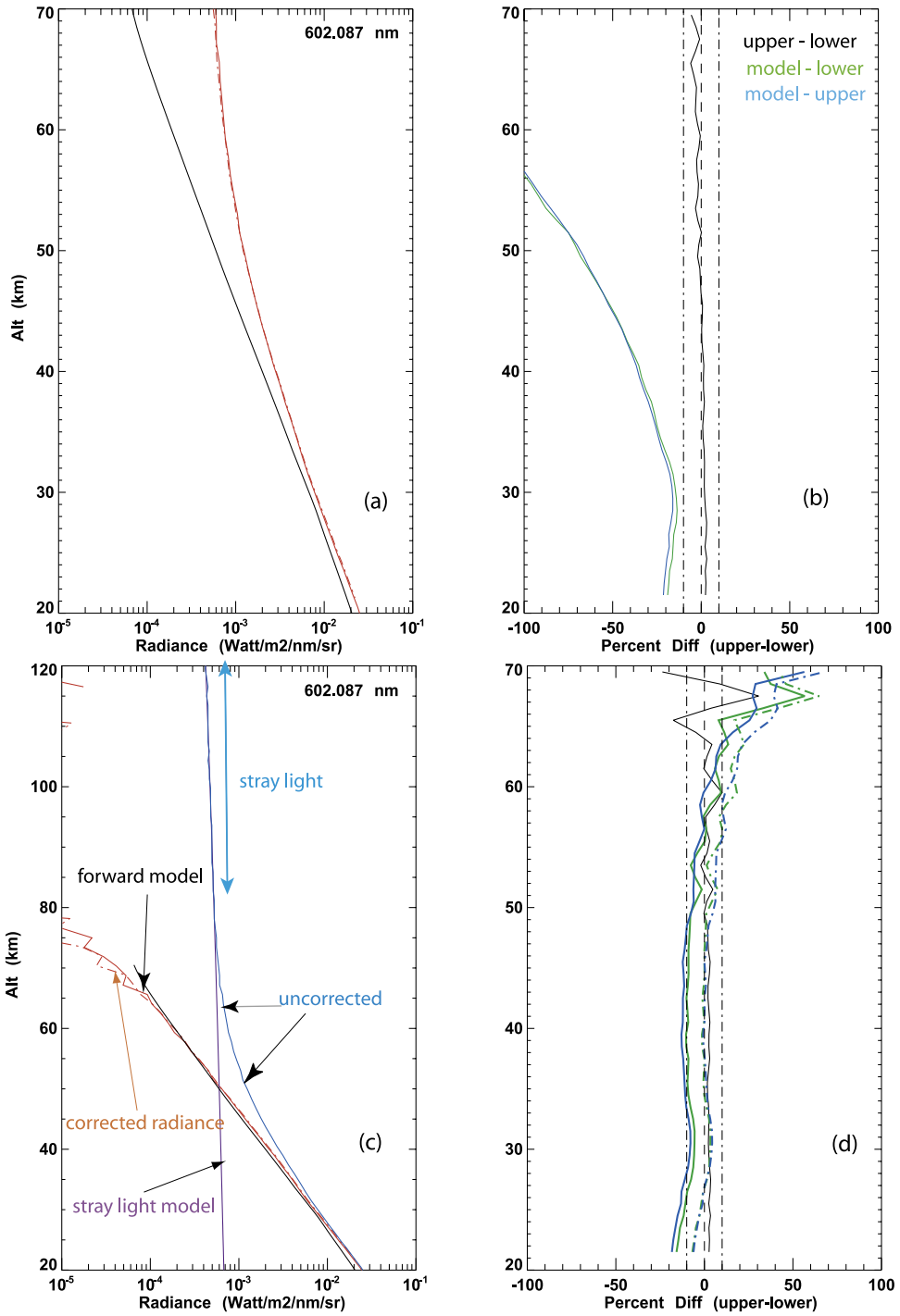

Figure 3. (a) Plot of forward model simulation (black) and measured GOMOS radiances (red dash-dotted, upper band; red solid, lower band) at a wavelength of 600 nm and no stray light corrections. (b) The percent difference between the GOMOS-measured upper and lower bands (black), the model and the lower band (green), and the model and the upper band (blue). (c) Same as Figure 3a but with an expanded *x* axis up to 120 km. GOMOS measurements here are shown in blue. The straight line (violet) is the stray light model. GOMOS upper and lower measurements (red) shown here are corrected for stray light. (d) Same as Figure 3b but for corrected GOMOS measurements for stray light. Also shown is the percent difference of normalized and corrected radiances (dash-dotted). Same color as Figure 3b.

tion in some measurements, dominate the mean difference at wavelengths between 350 and 500 nm. Errors due to inaccurate aerosol modeling are negligible above 25 km.

[10] *Flynn et al.* [2006] show that modeled radiances at 600 nm using ground reflectivity of $A = 0.2$ and $A = 0.8$ differ by 25 and −25% from the $A = 0.5$ case prior to normalization. Normalizing radiances at a reference altitude

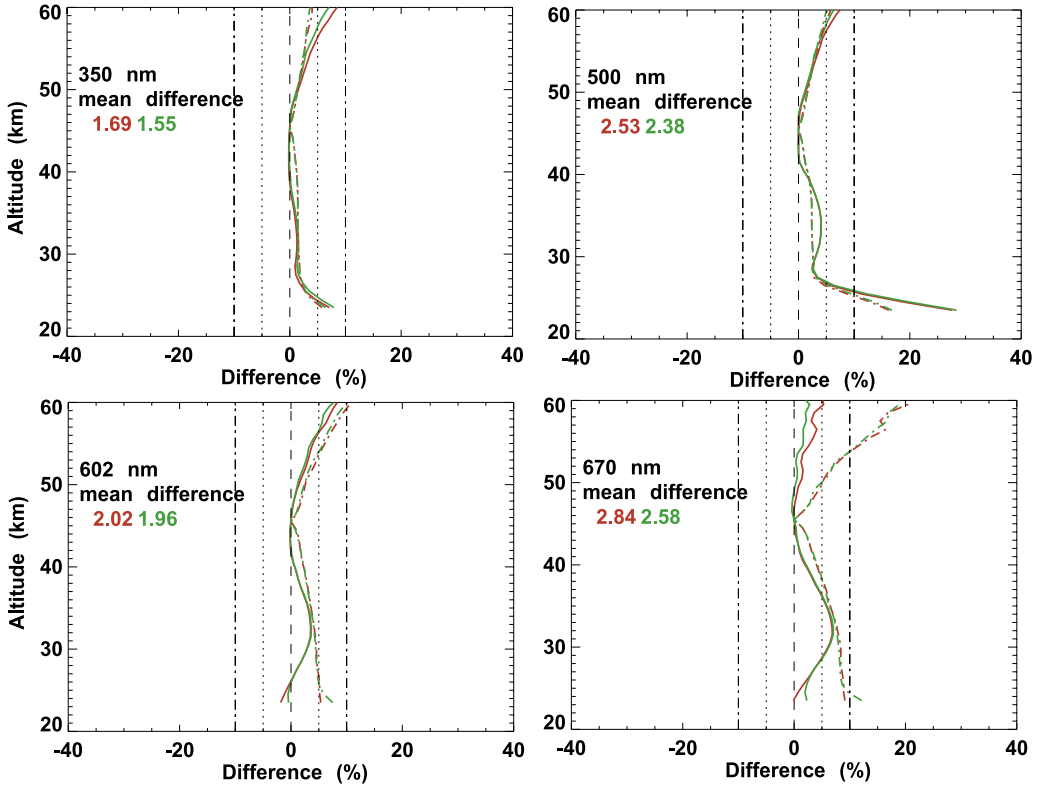

Figure 4. Plot of the mean difference for all events (98 events) of measured and calculated normalized radiances at 350, 500, 602, and 670 nm. The solid lines are the mean differences for upper (red) and lower (green) bands. The dash-dotted lines are the standard deviation of the means. Also shown in red and green is the mean difference over an altitude range of 22–50 km.

(42 km) and forming a triplet with 525 and 675 nm reduces the difference to less than 3%. Their conclusion was that error in a modeled reflectivity should have little impact on the accuracy of a modeled triplet used for ozone retrieval.

[11] Our analysis indicates an increase of retrieved ozone by 3% when changing the albedo from 0.05 to 0.8. If a value of $A = 0.3$ is used instead of 0.05, the increase is 1%. The albedo effect is almost negligible for UV wavelengths. This is consistent with *Rault and Taha* [2007], who used SAGE III limb measurements to show that a change of surface reflectance from 0.5 to 0.05 would lead to a retrieved ozone density increase of ~3–5% near the ozone maximum. Similarly, *von Savigny et al.* [2005a] performed a sensitivity analysis using OSIRIS measurements and concluded that the systematic errors in the retrieved ozone density introduced by an incorrect albedo are smaller than 1.5% between 15 and 40 km.

4. Altitude Registration

[12] Limb scattering experiments generally suffer from inaccurate pointing knowledge and must rely on scene-based algorithms to derive tangent height registration. The techniques used include a Rayleigh scattering attitude sensor (RSAS) [*Rault*, 2005] and ozone knee [*von Savigny et al.*, 2005b]. On the other hand, GOMOS measurements are known for their highly accurate altitude registration, better than ±50 m [*Borchi and Pommereau*, 2007]. The altitude of the measurement is defined by the direction of the star and the position of the spacecraft. The GOMOS ground processing derives its tangent height information using precise knowledge of the satellite location and a pointing system that includes a steering front mechanism and a star tracker unit that accurately points the instrument toward a selected star [*Paulsen et al.*, 1999]. Therefore, GOMOS limb scattering measurements should provide valuable tools to test, validate, and optimize scene-based tangent height registration algorithms.

[13] A scene-based knowledge of tangent high registration is usually inferred directly from measured radiances at selected wavelengths when compared with a forward model at those wavelengths. Generally, selected wavelength and altitude regions are influenced by ozone and exhibit vertical "knee" features at 300–310 nm [*Sioris et al.*, 2003; *Kaiser et al.*, 2004] or by Rayleigh extinction around 350 nm, known as the RSAS [*Janz et al.*, 1996; *Rault*, 2005].

[14] To analyze GOMOS pointing, a set of 20 pixels were selected (348–353 nm) where Rayleigh extinction has the dominant effect on the vertical radiance profile. After correcting for stray light, the measured radiances are compared to forward model radiances, generated as described in section 3. An altitude offset is derived by introducing a set of 10 m offsets, up to ±2 km, and searching for the maximum correlation coefficient. The comparison is made over the 25–50 km altitude range (just above the signal saturation altitude).

[15] Figure 5 is a plot of the comparison for a single profile. The left plot shows all measured (20 upper and

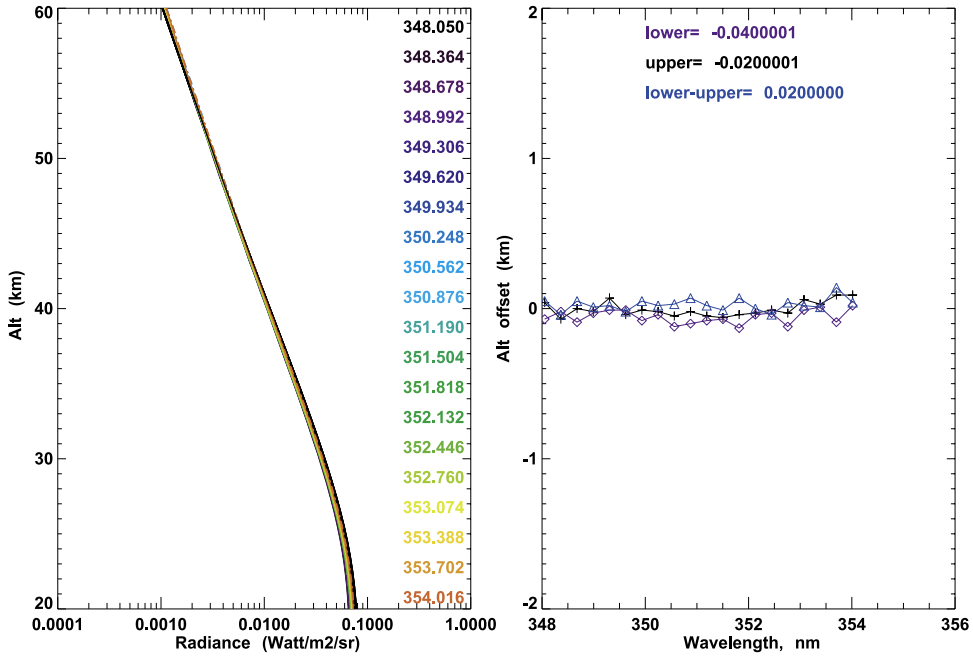

Figure 5. A plot of altitude registration analysis for a single event. (left) All measured (upper (dash-dotted) and lower (solid)) 20 pixels, colored by wavelength, and the calculated radiances (black). (right) A plot of the derived altitude offset at each pixel for both upper (black) and lower (violet) radiances. Also shown is the offset detected between the measured lower and upper (blue) bands.

20 lower) pixels, colored by wavelength, and the calculated radiances (black). The right plot is one of the derived altitude offset at each pixel for both upper (black) and lower (violet) radiances. Also shown is the detected offset between the measured lower and upper bands (blue). The lower-upper offset provides an indication of the error sources of this technique. The offset is the median of all 20 pixels. For this profile, the derived offset for the upper and lower bands is −40 and −20 m, respectively. The lower-upper band offset is 20 m.

[16] Figure 6 is a histogram that summarizes the distribution of all detected offsets for all profiles. Figure 6 is more representative of the accuracy of the technique used to derive altitude registration. The left plot is a histogram of the lower-upper offset, the right plot is for the upper band, and the middle plot is for lower band. The numbers shown are the mean and standard deviation of the offsets. The detected mean offsets were −27 and −44 m for lower and upper bands, respectively. The standard deviation for both bands was ∼350 m. The lower-upper offset is 54 m, and the standard deviation is 74 m.

[17] The derived mean offsets for both upper and lower bands are consistent with each other and with the ±50 m reported accuracy of GOMOS altitude registration. The 350 m standard deviation reflects GOMOS pointing uncertainties, as well as uncertainties associated with this technique, such as instrument and modeling errors. Modeling errors are mainly caused by inaccurate temperature and

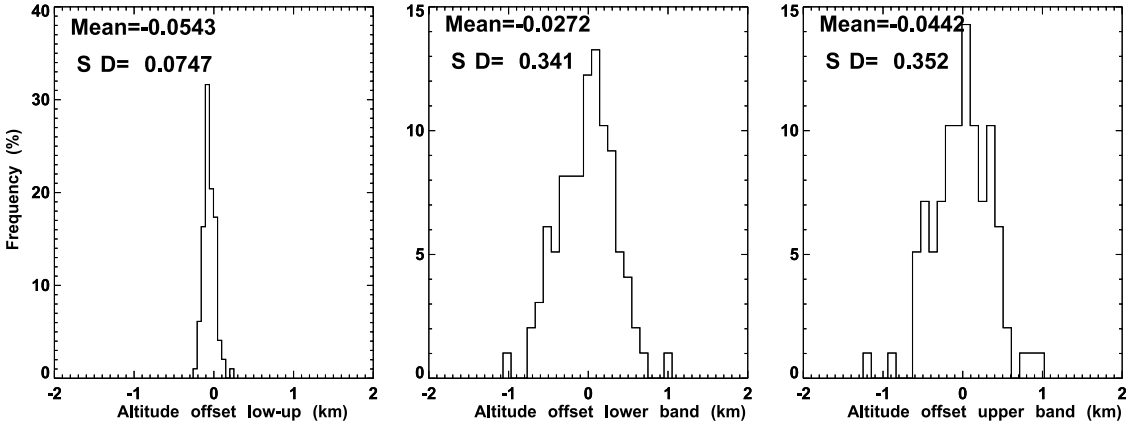

Figure 6. Summary histogram showing the distribution for all detected offsets of GOMOS events. (left) A histogram of lower-upper offsets (km). (right) A histogram of the upper band offsets. (middle) A histogram for the lower band. Also shown are the mean and standard deviation of the observed offsets.

aerosol profiles. Signal saturation results in a significant error by limiting the altitude range where the comparison is made, in some cases, to an altitude above the maximum curvature. The effect of stray light contamination is small since the maximum altitude range was restricted to 50 km, where stray light is negligible for the selected wavelengths. Turning off stray light corrections only resulted in ~10 m mean difference. *Rault and Taha* [2007] derived an average standard deviation of 350 m using the modified RSAS technique and comparing SAGE III LS ozone profiles to various correlative measurements.

[18] To test the ozone knee approach, we applied the same technique as for RSAS but used different GOMOS pixels (312–315 nm). The detected altitude offset was ~600 m with a standard deviation of ~350 m. A bias of 500 ± 500 m was reported by *Rault* [2005] when he compared SAGE III LS altitude registration using a modified RSAS with an ozone knee method. The main source of error for the ozone knee is the ozone profile used to run the forward model. Given that a SAGE II profile is used to simulate radiances at each GOMOS measurement location, which is known to be accurate up to 55 km [*Rault and Taha*, 2007], and the fact that the ozone knee for the selected wavelengths was always below 50 km, we believe that this error is small. The 600 ± 350 m bias is at odds with the accurate GOMOS pointing, indicating a modeling error for those wavelengths, and requires further investigation. The forward model calculations were repeated using different ozone cross sections; however, differences were small and did not explain the bias. Stray light contamination is very small for the selected wavelength and altitude ranges.

5. Retrieval Algorithm

[19] The OMPS algorithm performs a simultaneous optimal estimation inversion of both Hartley-Huggins and Chappuis band radiances, as outlined by *Flittner et al.* [2000], who described the ozone retrieval algorithm used for the Shuttle Ozone Limb Scattering Experiment–Limb Ozone Retrieval Experiment. The retrieval was further applied to OSIRIS measurements by *von Savigny et al.* [2003]. Each limb radiance profile is normalized by measured radiance at a reference altitude, typically in the range 60–45 km and depending on sensitivity to O_3 absorption and radiance quality. Normalization serves to self-calibrate the signal in much the same way that the unattenuated solar signal is used in solar occultation measurements. It also reduces the effect of surface reflectance and clouds [*Flittner et al.*, 2000]. The retrieval uses the ratio of two spectral channels in the UV range, a strong and a weak O_3 absorption, and a triplet for the visible wavelengths, one strong wavelength divided by the average of two weaker ozone-absorbing wavelengths. The triplet is designed to minimize the effect of aerosol scattering.

[20] The retrieval is performed using an optimal estimation scheme [*Rodgers*, 2000], described as

$$x_{n+1} = x_0 + \left(K_n^T S_y^{-1} K_n + S_a^{-1}\right)^{-1} K_n^T S_y^{-1}[(y - y_n) - K_n(x_0 - x_n)].$$

In this equation x_{n+1} is the ozone profile after $n + 1$ iterations, x_0 is the a priori profile, S_a is the a priori covariance matrix, S_y is the covariance matrix of the measured radiance y, and y_n is the calculated limb radiance. The weighting function or kernel K_n, describes the sensitivity of the calculated radiances with respect to the state vector x_n. The elements of K are defined as

$$K_{ij}|_n = dy_i/dx_j|_n,$$

where i is the index of the wavelength channel and j is index of altitude level. The retrieval is best characterized by studying the averaging kernel matrix A_k, which describes the sensitivity of the retrieval to the true state:

$$A_k = DK,$$

where D is the gain or (contribution) matrix, which describes the sensitivity of the retrieval to the measurements,

$$D = \left(K_n^T S_y^{-1} K_n + S_a^{-1}\right)^{-1} K_n^T S_y^{-1}.$$

[21] In the UV range, pixels at wavelengths 299, 302, 310, and 320 nm were paired with either 347 or 353 nm and normalized at ~53.5 km. Radiances used in the retrieval are restricted to an altitude range of 38–54 km. For the visible channels, pixels at wavelengths 575, 602, and 616 nm were paired with 514 and 675 nm, normalized at ~45.5 km, and restricted to an altitude range from 22 to 38 km. Different combinations of doublets and triplets were tried, and the ones reported here produced the best result. The code in its current version is flexible enough to change the wavelength selection and normalization altitude. Ideally, the code should utilize the measurement uncertainties to optimally weigh the wavelength pairs and to best select the normalization altitude in order to optimize the retrieval. The radiance uncertainties reported for GOMOS assume only simple Gaussian counting statistics and do not reflect the actual measurement uncertainty. The GOMOS measurements errors are dominated by saturation and stray light that varies with altitude and wavelength. Instead, a set of constant values of signal to noise ratio S/N over the retrieved altitude range that resulted in near-unity averaging kernels were used in the retrieval.

[22] In this work, we use the same single ozone profile as a priori for all retrievals to ensure minimum influence on the solution. A constant ground albedo of $A = 0.05$ is assumed for all retrievals. SAGE II NO_2 and aerosol profiles were also used, and a stratospheric sulfate aerosol is assumed. *Rault and Taha* [2007] showed that aerosol contribution is only significant below 25 km, while neglecting NO_2 would lead to less than 3% O_3 error.

6. Results and Discussion

[23] In this section, we present the retrieved ozone profiles using GOMOS limb scattering and compare them to SAGE II measurements. During the year 2003, GOMOS performed more than 140,000 vertical profile scans, 45% of which were daylight observations. In this work, 98 GOMOS bright limb profiles (SZA less than 85°) were selected. Each profile includes two background measurements, upper and lower. Furthermore, measurements were selected to coincide

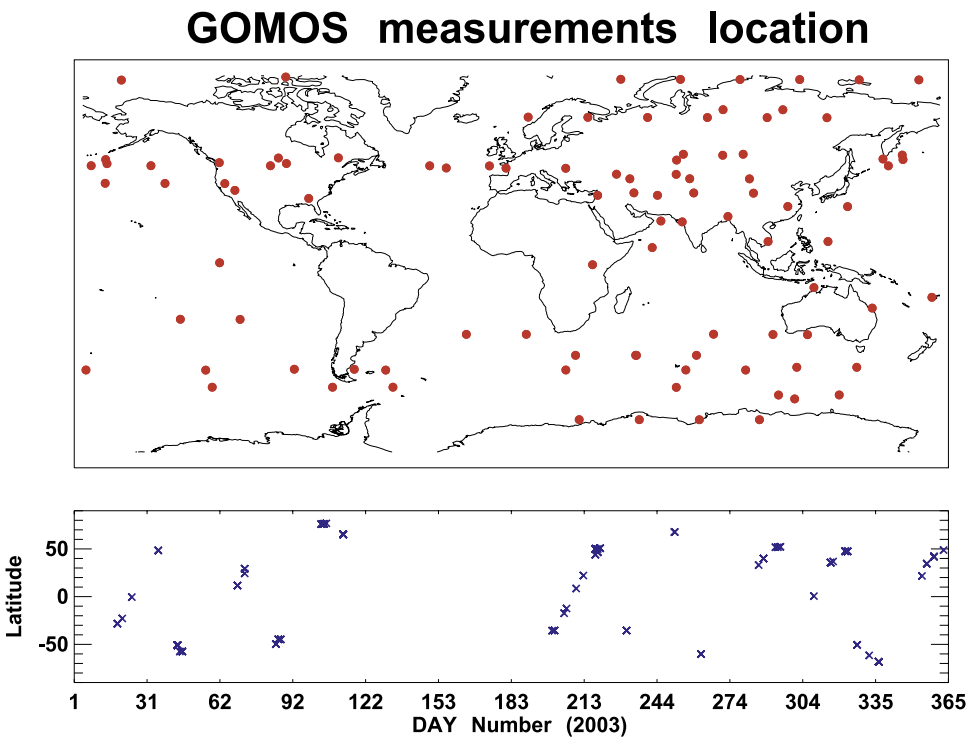

Figure 7. Location of GOMOS measurements (top) subset and (bottom) latitude versus time.

with SAGE II [*Chu et al.*, 1989], within 150 km and on the same day. The selected data set is evenly distributed around the globe and in time. Figure 7 is a measurement location map. The bottom plot is a scatterplot of each measurement's latitude versus time. SAGE II has been the benchmark for satellite ozone profile measurements in the stratosphere and is widely known for its highly accurate and precise measurements. The reported accuracy is ~5% in the altitude range 15–45 km, and the precision is as low as 2% down to 20 km [*Wang et al.*, 2002; *Borchi et al.*, 2004].

[24] Figure 8 is a typical ozone profile retrieval for a single measurement profile, the same event as investigated

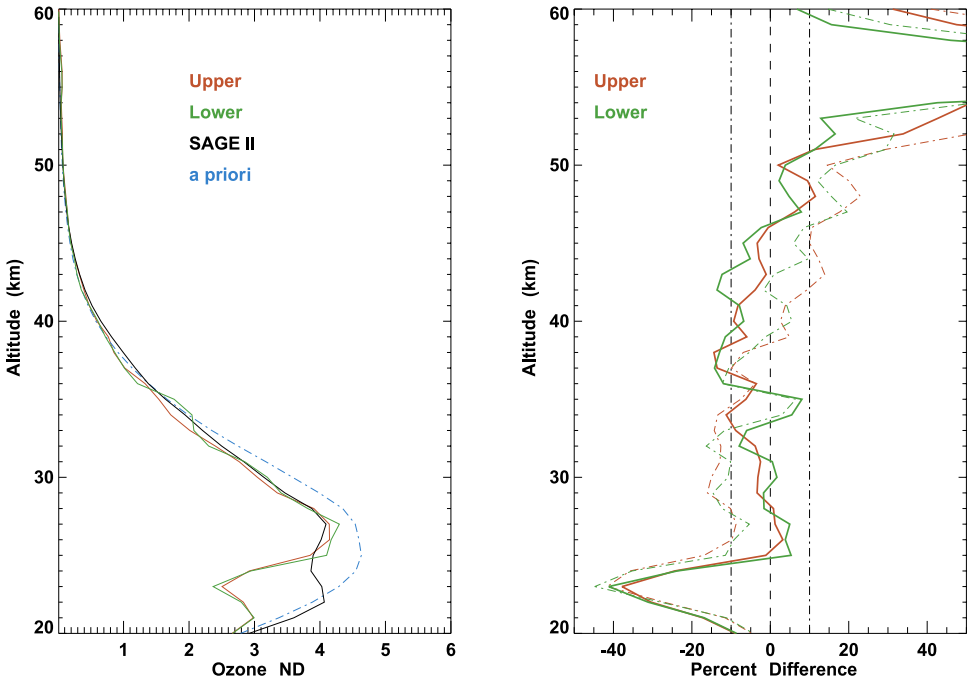

Figure 8. (left) The retrieved ozone profile number density ($\times 1^{12}$ cm^{-3}) for upper (red) and lower (green) bands. Black is SAGE II ozone profile, while blue is the a priori profile. (right) The percent difference between the retrieved ozone profiles for upper and lower bands and SAGE II. The dash-dotted lines are the difference of GOMOS versus a priori.

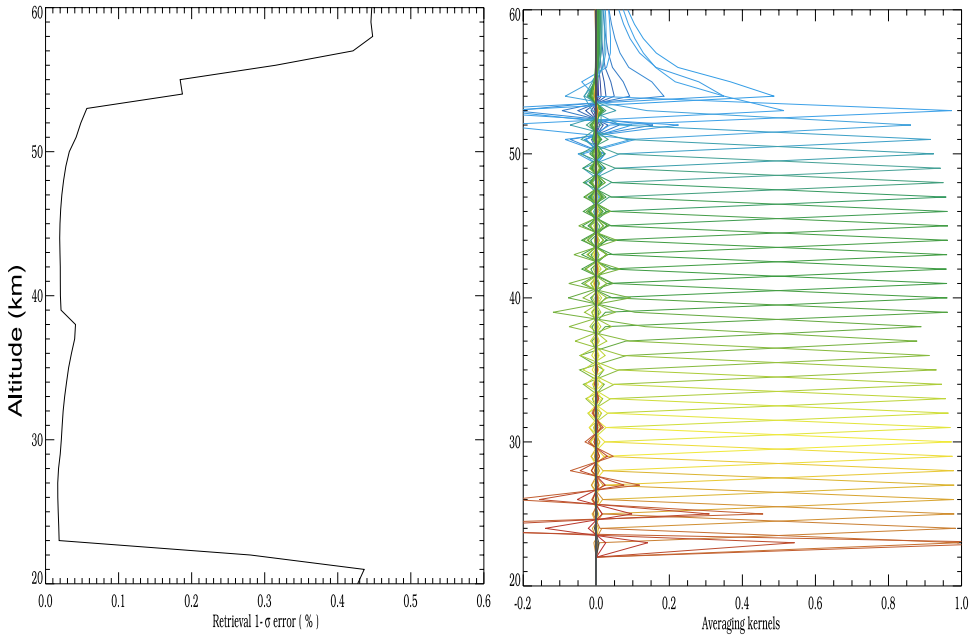

Figure 9. Plot of (left) the 1σ retrieval error in percent and (right) averaging kernel for the same retrieved ozone profile as in Figure 5 (upper band).

in section 2. The left plot is the retrieved ozone profile for upper (red) and lower (green) bands. Black is the SAGE II ozone profile, while blue is the a priori profile. The right plot is the difference between the retrieved ozone profiles for upper and lower bands and SAGE II in percent. The dash-dotted lines are the difference of GOMOS and the a priori profile. Figure 8 shows consistent retrieval for both upper and lower bands. Although upper and lower measurements are made separately, they are expected to agree to within instrument noise since they are very close in location. The observed differences between retrieved ozone and SAGE II values are mostly within ±10% in the altitude range of 25–50 km. Below 25 km, the retrieval is unrealistic as a result of signal saturation. The saturated pixels have no effect on the retrieval at other altitudes. The percent difference at the altitude range 34–43 km is greater but still within 10%. This is the altitude range where the transition between UV and visible wavelength retrieval takes place and ozone absorption is weaker. Above 50 km, the retrieval is also unrealistic, mainly because of decreased measurement sensitivity and the increased instrument noise.

[25] Figure 9 is a plot of 1σ retrieval errors (left) and averaging kernel (right) for the same retrieved ozone profile as in Figure 5 (upper band). The 1σ retrieval error is based on the inversion algorithm covariance matrix, which mainly reflects retrieval algorithm sensitivity, forward model error, and measurement noise. The measurement noise does not include signal saturation or stray light contamination, the dominant sources of uncertainty for GOMOS limb measurements. The retrieval error is less than 5% at the altitude region 23–53 km. The error increases significantly to more than 40% outside this altitude range. Similarly, the averaging kernels are close to unity over the same altitude range, indicating excellent information content from the measurements and, hence, little dependence of the retrieved profile on a priori information. Notice that the 1σ retrieval error is too low as it is yet to include several instrument and modeling uncertainties.

[26] The coincidences between SAGE II and GOMOS were divided into three latitude bands, southern ($-80° \leq$ latitude $< -30°$), equatorial ($-30° \leq$ latitude $\leq 30°$), and northern ($30° <$ latitude $\leq 80°$). In addition, the data were divided into four seasons: December-January-February, March-April-May, June-July-August, and September-October-November. The sample number is too small to make any statistically significant findings; however, it is a useful tool for identifying any area of enhanced biases or retrieval breakdown at various atmospheric conditions. A larger number of events are needed to provide a robust assessment of any systematic seasonal or geographical biases.

[27] Figure 10a contains the detailed results of the comparison between GOMOS and SAGE II during 2003. It shows the mean ozone profile number density for SAGE II (black) and GOMOS upper (red) and lower (green) bands. The error bars are the standard deviation. Also shown are the latitude range, months, and number of profiles used in each comparison. Figure 10b is the corresponding percent difference between retrieved GOMOS profiles and SAGE II. The dash-dotted lines are the standard deviation of the difference. On the right side is the number of valid measurements included in calculating the average. Also shown is the mean bias, which is the mean of the difference over the altitude range of 25–50 km for both upper and lower band retrievals. The average difference and standard deviation are calculated using only data points that were within 30% of SAGE II measurements. This filter was necessary to exclude corrupted and unrealistic outliers without influencing the real differences observed between GOMOS and SAGE since the algorithm in its current version does not flag for those erroneous retrievals. Most of the excluded measurements are below 27 km and result from signal saturation. Some measurements were also excluded around 38 km, the

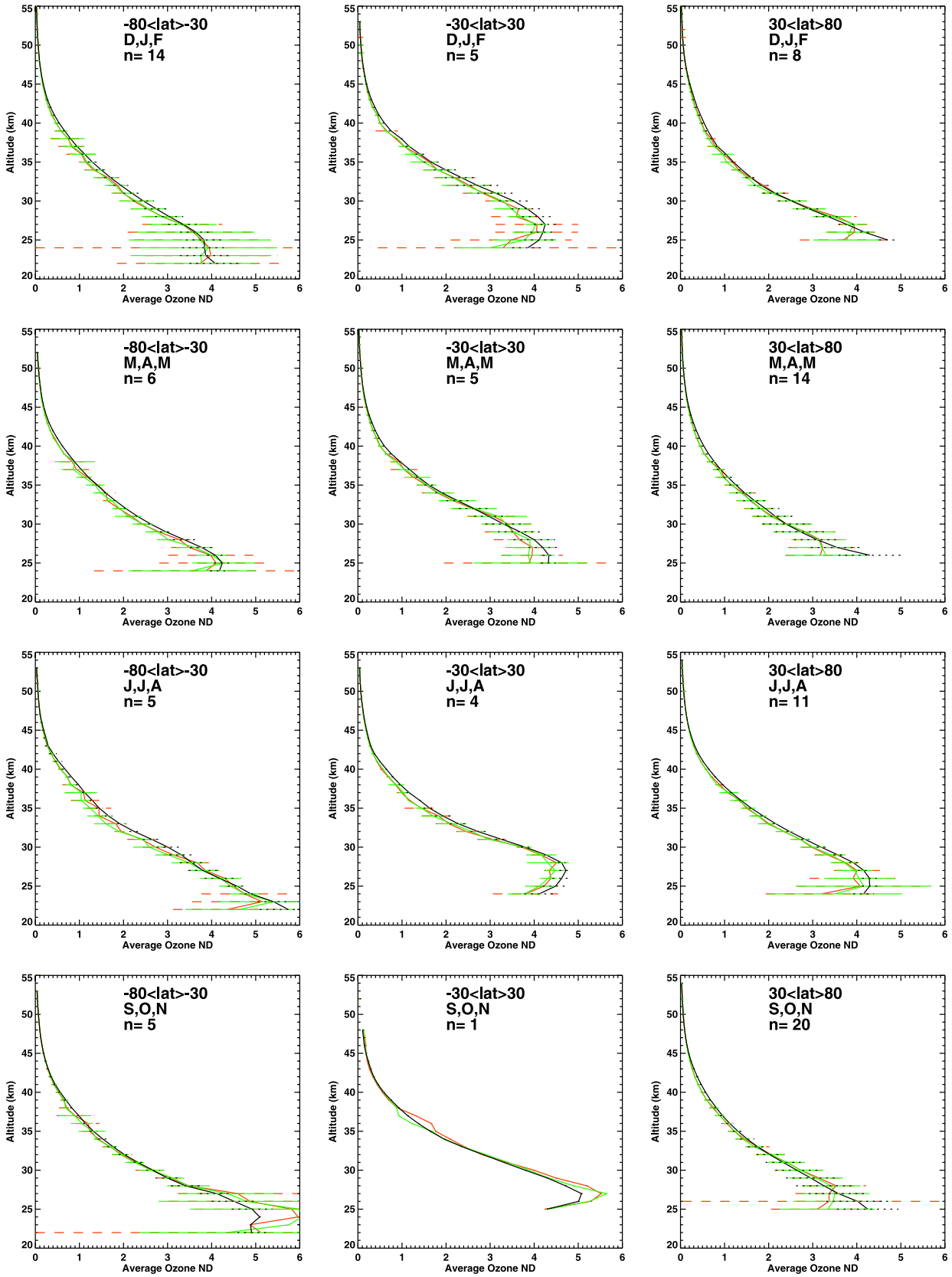

Figure 10a. Detailed result of comparisons between GOMOS and SAGE II during 2003, divided into 12 latitude-season categories. It shows the mean profiles of SAGE II and GOMOS upper (red) and lower (green) bands. The error bars are the standard deviation. Also shown are the latitude range, months, and number of profiles. D, J, F, December, January, February; M, A, M, March, April, May; J, J, A, June, July, August; S, O, N, September, October, November.

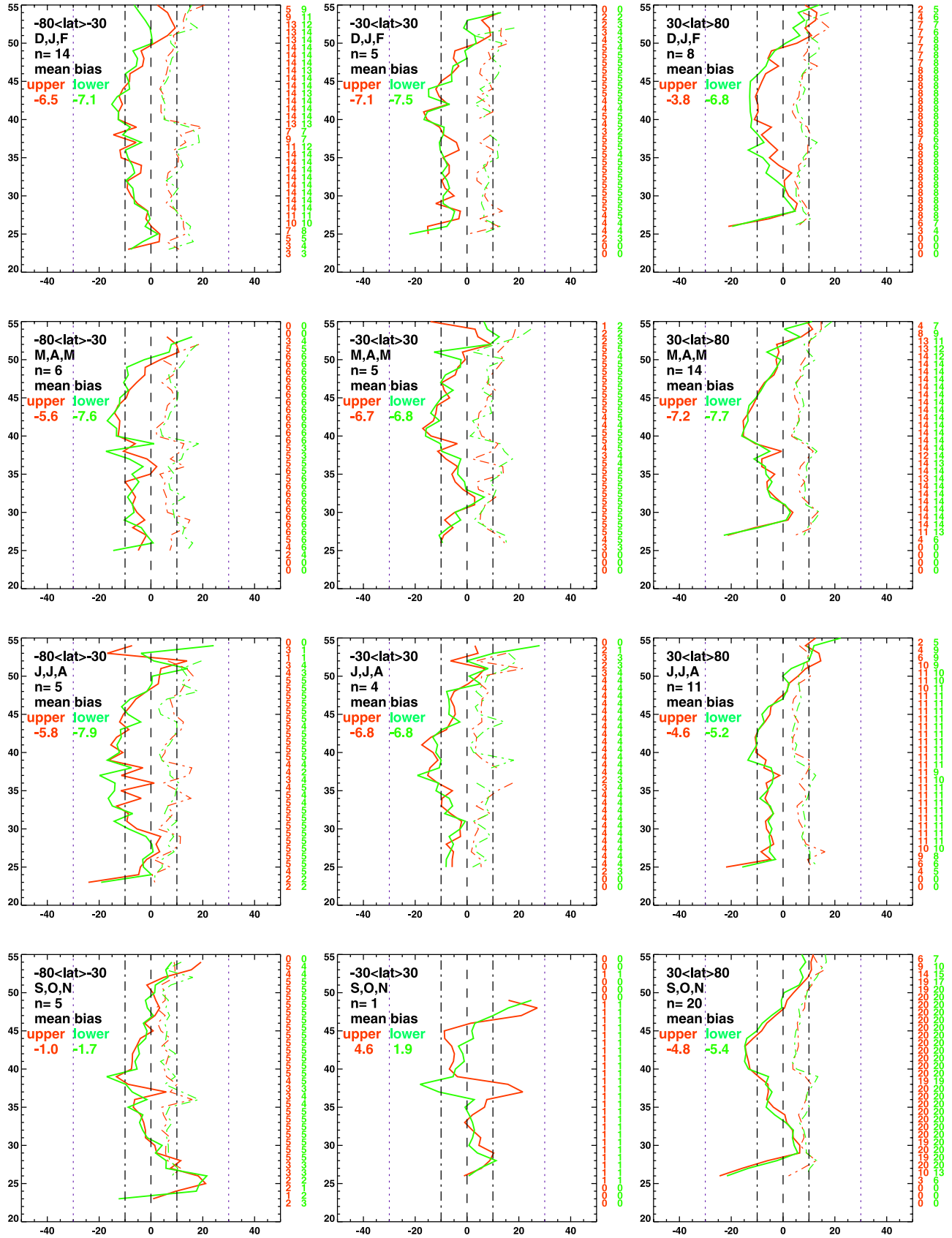

Figure 10b. Same as Figure 10a but for the mean difference. The dash-dotted lines are the standard deviation. Also shown in red and green is the mean bias over altitude range 25–50 km.

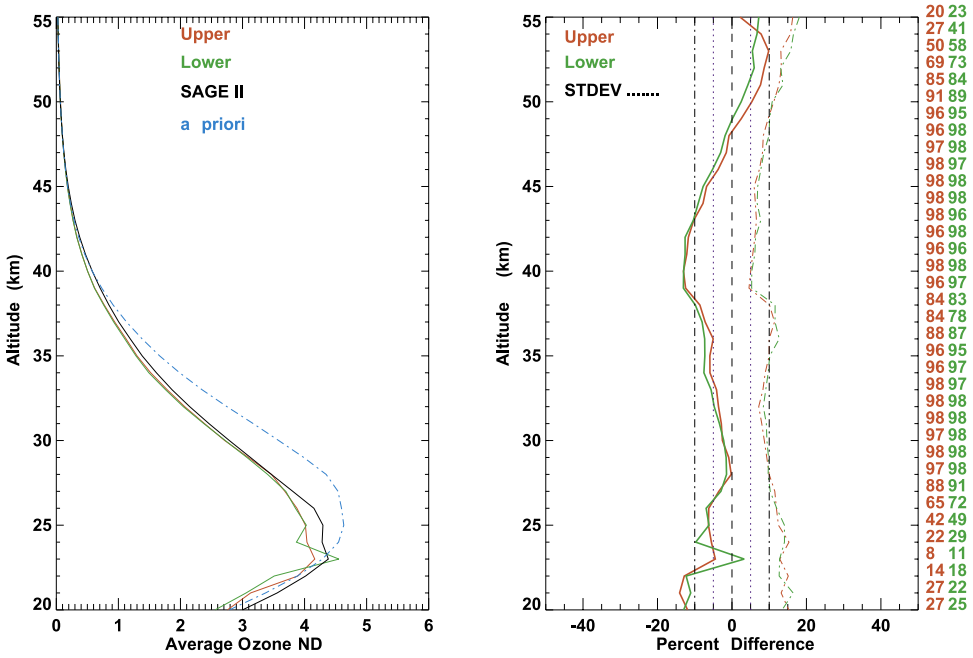

Figure 11. Same as Figure 8 but for the average of all coincidences. The red and green numbers on the right plot are the number of measurement points included in the comparison.

altitude where the transition between UV and visible channels takes place. Differences between UV and visible retrievals result in inconsistencies that the code cannot currently reconcile. Generally, the retrieved ozone profiles only reached down to the peak of the ozone layer in the equatorial latitudes. Our statistical sample is too small to draw any conclusion about seasonal or geographical biases. However, it demonstrates consistent retrieval biases under different atmospheric conditions. It also shows that GOMOS retrieved ozone profiles capture the same latitudinal-seasonal dependencies exhibited by SAGE II. The average mean difference is mainly within 10%. However, at altitude range 38–43 km, the difference is ~15%. The standard deviation is also within 10%. The retrieved profiles show enhanced variability below 28 km, which is caused by an increasing percentage of saturated pixels at lower altitudes. Overall, the mean bias is approximately −7% for the comparison and is consistent for both upper and lower retrievals, which are within 1–2% of each other.

[28] Figure 11 is a summary plot of all the comparisons for retrieved GOMOS ozone profile number density. It is the same as Figure 8 but is for the average of all comparisons (98 events). On the right plot are the numbers of measurement points included in the comparison. The observed percent difference is within 10% over the altitude range 24–50 km. An enhanced difference of ~15% can be seen at 38–40 km altitude range. The agreement is better below 35 km. The standard deviation is almost unchanged for all altitudes, ~7–10%. Both upper and lower band retrieved ozone profiles show consistent behavior. Retrievals outside the altitude range of 22–52 km are heavily weighted toward the a priori.

[29] The observed bias between GOMOS and SAGE II can be in part explained by instrument and modeling uncertainties. Stray light mitigation measures applied to GOMOS radiances manage to reduce the uncertainty to less than 3% for visible pixels. Stray light contamination is very small at UV wavelengths. Saturation is limited to lower altitudes and can result in unrealistic retrievals, which explains the increased standard deviation and decreased valid measurement points below 28 km. Surface albedo error is expected to be ~3% and is negligible above 38 km, while NO_2 error is less than 1% near its peak. Aerosol profile uncertainty is negligible for altitudes above 25 km. The effect of line-of-sight inhomogeneity is more complex, and further studies are needed for a better uncertainty estimate. Altitude registration errors are minimal because of the GOMOS stellar pointing information. A fraction of the retrieved O_3 difference is real, caused by instrument differences and atmospheric variability. Enhanced differences observed at 38–40 km are mainly caused by differences of UV and visible retrievals. Since ozone cross sections are sensitive to temperature at the UV wavelength, temperature inaccuracies at these altitudes contribute to the enhanced difference. Also, the kernels of both UV and Chappuis wavelengths are smaller for this altitude region. SAGE III LS ozone showed similar behavior of increased differences when switching to UV wavelength retrievals [*Rault and Taha*, 2007]. Those differences were attributed to the decrease in instrument signal and the increase in retrieval uncertainties. Further work is needed to understand the origin of the crossover region differences and is the best approach for merging UV and visible information, such as retrieving separate UV and Chappuis profiles, similar to SAGE III [*Rault*, 2005], or using a differential optical absorption spectroscopy like retrieval, where it is possible to analyze the spectral dependence of the residuals in order to understand and further quantify both instrument and modeling errors.

[30] These retrieved ozone profiles demonstrate a good potential for GOMOS bright limb measurements and are comparable to those of SAGE III limb measurements of 5–10% [*Rault and Taha*, 2007]; 6% for SCIAMACHY [*Brinksma et al.*, 2006]; and 7% in the altitude range 15–32 km, 15% above 32 km for OSIRIS [*Petelina et al.*, 2004]. SCIAMACHY and OSIRIS use only the Chappuis band, which restricts the upper limit of the retrieved ozone profile to 36 km. Recent results of SCIAMACHY retrieved ozone in the Hartley bands is mainly within 10% of correlative measurements [*Rohen et al.*, 2007]. Further tuning of the retrieval algorithm and a more extensive validation analysis using more instruments and a larger statistical sample would benefit the retrieval by further understanding and quantifying the retrieval uncertainties.

7. Summary and Conclusion

[31] GOMOS limb scattering measurements were analyzed and compared to radiances calculated using a forward model, with inputs from a nearby SAGE II measurement. Results show that GOMOS limb measurements suffer from signal saturation and stray light contamination. An empirical model to estimate the stray light signal was applied and shown to be effective in correcting GOMOS radiances up to ~60 km tangent altitude. GOMOS radiances were used to test a scene-based tangent height algorithm, and the best results were achieved using ~350 nm (Rayleigh) pixels that were consistent with GOMOS known accurate pointing. The corrected radiances were also used to retrieve ozone number density profiles, which were compared to SAGE II. Ozone retrievals were restricted to ~25–50 km because of signal saturation and residual stray light. The retrieved ozone profiles using GOMOS bright limb measurements have been demonstrated to have a good potential, as initial results show; in general, an agreement with collocated SAGE II measurements to within 10–15%; and a standard deviation of ~10% and were consistent for both upper and lower bands. The accuracy of these retrievals is comparable to similar limb scattering instruments, such as SAGE III LS, SCIAMACHY, and OSIRIS.

[32] In this initial work, we showed that the GOMOS upper and lower band measurements, if properly corrected for stray light signal, contain very useful information of the ozone number density profile and can supplement the stellar occultation routine production to provide near-global coverage. Our results illustrate the good potential for GOMOS limb scattering measurements; however, further analysis and improvement of the retrieval algorithm should improve the quality of such measurements.

[33] **Acknowledgments.** The authors would like to acknowledge valuable discussions and comments with D. Flittner, D. Rault, W. Qin, and B Wenny. We would also like to acknowledge valuable remarks given by anonymous reviewers. Thanks to ACRI, ESA, and the GOMOS team for providing GOMOS level 1b data used in this study and for the SAGE II team at NASA LaRC for processing SAGE II version 6.2 measurements. This work was supported by NASA contract NNG06HX18C.

References

Borchi, F., and J.-P. Pommereau (2007), Evaluation of ozonesondes, HALOE, SAGE II and III, Odin-OSIRIS and -SMR, and Envisat-GOMOS, -SCIAMACHY and -MIPAS ozone profiles in the tropics from SAOZ long duration balloon measurements in 2003 and 2004, *Atmos. Chem. Phys.*, *7*, 2671–2690.

Borchi, F., J.-P. Pommereau, A. Garnier, and M. Pinharanda (2004), Evaluation of SHADOZ sondes, HALOE and SAGE II ozone profiles at the tropics from SAOZ UV-vis remote measurements onboard long duration balloons, *Atmos. Chem. Phys. Disc.*, *4*, 4945–4997.

Bovensmann, H., J. P. Burrows, M. Buchwitz, J. Frerick, S. Noël, V. V. Rozanov, K. V. Chance, and A. P. H. Goede (1999), SCIAMACHY: Mission objectives and measurement modes, *J. Atmos. Sci.*, *56*(2), 127–150.

Brinksma, E. J., et al. (2006), Geophysical validation of SCIAMACHY limb ozone profiles, *Atmos. Chem. Phys.*, *6*, 197–209.

Chu, W. P., M. P. McCormick, J. Lenoble, C. Brogniez, and P. Pruvost (1989), SAGE II inversion algorithm, *J. Geophys. Res.*, *94*, 8339–8351, doi:10.1029/JD094iD06p08339.

European Space Agency (ESA) (2007a), GOMOS product handbook issue 3.0, technical report, Washington, D. C. (Available at http://envisat.esa.int/pub/ESA_DOC/ENVISAT/GOMOS/gomos.ProductHandbook.3_0.pdf)

European Space Agency (ESA) (2007b), GOMOS algorithm theoretical basis document version 2.0, technical report, Washington, D. C. (Available at http://envisat.esa.int/instruments/gomos/atbd/GOMOS_ATBD_v2.pdf)

Flittner, D. E., P. K. Bhartia, and B. M. Herman (2000), O_3 profiles retrieved from limb scatter measurements: Theory, *Geophys. Res. Lett.*, *27*, 2601–2604, doi:10.1029/1999GL011343.

Flynn, L. E., C. J. Seftor, J. C. Larsen, and P. Xu (2006), The Ozone Mapping and Profiler Suite, in *Earth Science Satellite Remote Sensing*, edited by J. J. Qu et al., pp. 279–296, doi:10.1007/978-3-540-37293-6, Springer, Berlin.

Herman, B. M., T. R. Caudill, D. E. Flittner, K. J. Thome, and A. Ben-David (1995), Comparison of the Gauss-Seidel spherical polarized radiative transfer code with other radiative transfer codes, *Appl. Opt.*, *34*, 4563–4572.

Janz, S. J., E. Hilsenrath, D. Flittner, and D. Heath (1996), Rayleigh scattering attitude sensor, *Proc. SPIE Int. Soc. Opt. Eng.*, *2831*, 146–153.

Kaiser, J. W., C. von Savigny, K.-U. Eichmann, S. Noel, H. Bovensmann, and J. P. Burrows (2004), Satellite pointing retrieval from atmospheric limb scattering of solar UV-B radiation, *Can. J. Phys.*, *82*, 1041–1052, doi:10.1139/p04-071.

Kyrölä, E., et al. (2004), GOMOS on Envisat: An overview, *Adv. Space Res.*, *33*, 1020–1028, doi:10.1016/S0273-1177(03)00590-8.

Llewellyn, E. J., et al. (2004), The OSIRIS instrument on the Odin spacecraft, *Can. J. Phys.*, *82*, 411–422, doi:10.1139/p04-005.

Meijer, Y. J., et al. (2004), Pole-to-pole validation of Envisat GOMOS ozone profiles using data from ground-based and balloon sonde measurements, *J. Geophys. Res.*, *109*, D23305, doi:10.1029/2004JD004834.

Paulsen, T., A. F. Popescu, G. Ratier, G. Uguen, and C. Lemercier (1999), The Global Ozone Monitoring by Occultation of Stars (GOMOS) instrument on Envisat, in *IGARSS '99 Proceedings: Remote Sensing of the System Earth—A Challenge for the 21st Century*, vol. 2, edited by T. I. Stein, pp. 1438–1440, Inst. Electr. Electr. Eng., Piscataway, N. J.

Petelina, S. V., et al. (2004), Comparison of the Odin/OSIRIS stratospheric ozone profiles with coincident POAM III and ozonesonde measurements, *Geophys. Res. Lett.*, *31*, L07104, doi:10.1029/2003GL019299.

Rault, D. F. (2005), Ozone profile retrieval from Stratospheric Aerosol and Gas Experiment (SAGE III) limb scatter measurements, *J. Geophys. Res.*, *110*, D09309, doi:10.1029/2004JD004970.

Rault, D. F., and G. Taha (2007), Validation of ozone profiles retrieved from Stratospheric Aerosol and Gas Experiment III limb scatter measurements, *J. Geophys. Res.*, *112*, D13309, doi:10.1029/2006JD007679.

Rodgers, C. D. (2000), *Inverse Methods for Atmospheric Sounding: Theory and Practice*, 238 pp., World Sci., Hackensack, N. J.

Rohen, G. J., et al. (2007), Ozone profile retrieval from limb scatter measurements in the HARTLEY bands: Methodology, algorithm description, sensitivity studies, and validation, *Atmos. Chem. Phys. Disc.*, *7*, 12,097–12,143.

Sioris, C. E., et al. (2003), Stratospheric profiles of nitrogen dioxide observed by Optical Spectrograph and Infrared Imager System on the Odin satellite, *J. Geophys. Res.*, *108*(D7), 4215, doi:10.1029/2002JD002672.

von Savigny, C., et al. (2003), Stratospheric ozone profiles retrieved from limb scattered sunlight radiance spectra measured by the OSIRIS instrument on the Odin satellite, *Geophys. Res. Lett.*, *30*(14), 1755, doi:10.1029/2002GL016401.

von Savigny, C., I. C. McDade, E. Griffioen, C. S. Haley, C. E. Sioris, and E. J. Llewellyn (2005a), Sensitivity studies and first validation of stratospheric ozone profile retrievals from Odin/OSIRIS observations of limb-scattered solar radiation, *Can. J. Phys.*, *83*, 957–972, doi:10.1139/p05-041.

von Savigny, C., J. W. Kaiser, H. Bovensmann, J. P. Burrows, I. S. McDermid, and T. Leblanc (2005b), Spatial and temporal characterization of SCIAMACHY limb pointing errors during the first three years of the mission, *Atmos. Chem. Phys.*, *5*, 2593–2602.

Wang, H. J., D. M. Cunnold, L. W. Thomason, J. M. Zawodny, and G. E. Bodeker (2002), Assessment of SAGE version 6.1 ozone data quality, *J. Geophys. Res.*, *107*(D23), 4691, doi:10.1029/2002JD002418.

D. Fussen and F. Vanhellemont, Belgian Institute for Space Aeronomy, Avenue Circulaire 3, B-1180 Brussels, Belgium. (didier.fussen@aeronomie.be; filip.vanhellemont@aeronomie.be)

G. Jaross and G. Taha, Science Systems and Applications Inc., Suite 500, 10210 Greenbelt Road, Lanham, MD 20706, USA. (glen.jaross@nasa.gov; ghassan_taha@ssaihq.com)

E. Kyrölä, Finnish Meteorological Institute, FIN-00101 Helsinki, Finland. (erkki.kyrola@fmi.fi)

R. D. McPeters, NASA Goddard Space Flight Center, Laboratory for Atmospheres, Code 613.3, Greenbelt, MD 20771, USA. (richard.d.mcpeters@nasa.gov)